Intrinsic coupled ocean-atmosphere modes of the Asian summer monsoon: A re-assessment of monsoon-ENSO relationships

K.-M. Lau and H. T. Wu

Climate and Radiation Branch

NASA/Goddard Space Flight Center

Greenbelt, MD 20771

(Submitted to J. Climate)

ABSTRACT

Using global rainfall and sea surface temperature (SST) data for the past two decades (1979-1998), we have investigated the intrinsic modes of Asian summer monsoon (ASM) and ENSO co-variability. Three recurring ASM rainfall-SST coupled modes were identified. The first is a basin scale mode that features SST and rainfall variability over the entire tropics (including the ASM region), identifiable with those occurring during El Niño or La Niña. This mode is further characterized by a pronounced biennial variation in ASM rainfall and SST associated with fluctuations of the anomalous Walker circulation that occur during El Niño /La Niña transitions. The second mode comprises mixed regional and basin-scale rainfall and SST signals, with pronounced intraseasonal and interannual variabilities. This mode features a SST pattern associated with a developing La Niña, with a pronounced low level anticyclone in the subtropics of the western Pacific off the coast of East Asia. The third mode depicts an east-west rainfall and SST dipole across the southern equatorial Indian Ocean, most likely stemming from coupled ocean-atmosphere processes within the ASM region. This mode also possesses a decadal time scale and a linear trend, which are not associated with El Niño /La Niña variability.

Possible causes of year-to-year rainfall variability over the ASM and sub-regions have been evaluated from a reconstruction of the observed rainfall from singular eigenvectors of the coupled modes. It is found that while basin-scale SST can account for portions of ASM rainfall variability during ENSO events (up to 60% in 1998), regional processes can accounts up to 20-25% of the rainfall variability in typical non-ENSO years. Stronger monsoon-ENSO relationship tends to occur in the boreal summer immediately preceding a pronounced La Niña , i.e., 1998, 1988 and 1983. Based on these results, we discuss the possible impacts of the ASM

on ENSO variability via the west Pacific anticyclone and articulate a hypothesis that anomalous wind forcings derived from the anticyclone may be instrumental in inducing a strong biennial modulation to natural ENSO cycles.

1. Introduction

The Asian summer monsoon (ASM) is subject to large interannual fluctuations resulting in floods and droughts of varying degree of severity in different ASM sub-regions. During the summer of 1998, the great flood over the Yangtze River was among one of the worst natural disasters on record (3700 deaths, 223 million people displaced and property damages up to $ US 30 billions). In the same year, excessive monsoon rainfall also caused severe flooding over Bangladesh (30 millions displaced and property damages up to 3.4 billion). Yet, one year before, in the summer of 1997, the above regions had nearly normal summer rainfall, but northern China experienced record drought, southern China was extremely wet with wide spread flooding, while the averaged rainfall over the entire India subcontinent was nearly normal. The above situation does not seem to be consistent with results of many previous studies which indicated a significant negative correlation between the El Niño Southern Oscillation (ENSO) and the Asian summer monsoon (Rasmusson and Carpenter 1983, Shukla and Paolino 1983, Webster and Yang 1992, Lau and Yang 1996, Ju and Slingo 1995 and many others). Various factors have been suggested to "explain" the discrepancies of the observed and the expected. These range from the possible impacts on monsoon rainfall anomalies by intraseasonal oscillations, the biennial oscillations, Indian Ocean sea surface temperature, Eurasian snow cover, decadal changes in ENSO monsoon coupling, to global warming. These factors have been the subject of a large number of recent investigations (Lau and Weng 2000, Webster et al 1999, Chandrasekar and Kitoh 1999, Shen and Kimoto 1999, Goswami et al. 1998, Li and Yanai 1996, Meehl and Arblaster 1998, Meehl 1997, Shen and Lau 1995 and many others). It is plausible that all these factors, to various degree, may have contributed to the ASM anomalies in 1997-98. However, a mere recognition of possible factors that may contribute to monsoon

anomalies, does not help with the understanding of monsoon-ENSO relationship and attribution of ASM anomalies, unless a methodology is developed so that the relative importance and the interrelationships among these factors can be quantified and evaluated.

One of the reasons for the aforementioned conundrum in identifying causes of ASM anomalies is that the monsoon-ENSO relationships obtained by previous studies were mostly based on indices, usually derived for a monsoon sub-region (e.g., the all-India monsoon rainfall index). Given the complexity and the vast region covered by the ASM, it is questionable that these sub-regional indices are appropriate measures of the broad-scale monsoon. Likewise, broad-scale monsoon indices (e.g. Webster and Yang 1992) that were used may not necessarily be applicable for regional and sub-regional monsoon variability. Recently, a number of investigators have pointed out the need to better define the regionality of the monsoon using different indices aimed at determinging regional monsoon climate variability (Goswami et al. 1999, Ailikun and Yasunari 1999, Wang and Fan 1999, and Lau et al. 2000). In particular, Lau et al. (2000) demonstrated that, based on the characteristics of dynamics and lower boundary forcings, at least two major subcomponents of the ASM, i.e., the South Asia monsoon (SAM) and the East-southeast Asia monsoon (EAM), need to be distinguished in monsoon-ENSO studies. In a pilot study to assess the regional impacts of the 1997-98 El Niño on the Asian-Australia monsoon, Lau and Wu (1999) found that both regional and basin-scale processes contributed significantly to the observed all-ASM rainfall anomalies in 1997. However, their paper did not address sub-regional scale rainfall variability such as those associated with SAM and EAM.

In this paper, we continue similar line of approach from Lau and Wu (1999), focusing on the quantitative evaluation of factors contributing to ASM rainfall variability. Unlike previous

monsoon-ENSO studies, which mostly viewed the monsoon from the vantage point of El Niño, here we re-examine the monsoon-ENSO relationship based on a "monsoon-centric" viewpoint. We will first compare and contrast the observed rainfall and SST anomalies in the ASM region, in the context of basin-scale variability of tropical rainfall and SST (Section 3). We then identify and provide physical interpretations to various recurring monsoon rainfall-SST modes using a number of comparative analyses (Sections 4). Next we use these modes to reconstruct the observed ASM rainfall anomalies, and to determine relative roles of various physical processes in accounting for the year-by-year observed rainfall anomalies (Section 5). Based on our findings, we also articulate a hypothesis on how the monsoon may impact the evolution of El Niño (Section 6). In this work, we shall only be concerned with SST-related rainfall anomalies. Land surface processes which are important for ASM variability will not be discussed.

2. Data and analysis procedure

We use rainfall, SST and wind for the present analysis. For rainfall, we used the CMAP monthly product with 2.5° x2.5° resolution for the period 1979- 1998 (Xie and Arkin 1997). For SST, we used the optimally gridded 2° x 2° product of Reynolds and Smith (1994) for the same period. Singular Value Decomposition (SVD) is used to identify the coupled patterns of rainfall and SST globally (40° S- 40° N), and over the ASM domain (20 °S-40° N, 30° E – 150° E) and different combinations of rainfall and SST domains to evaluate remote vs. regional SST forcings. While we focus on June-July- August (JJA) for the main discussions, we used the 5-month period from May through September (MJJAS) in the statistical analysis to include the extended boreal summer season and to increase the sampling. We use the wind products from the National Center for Environmental Prediction (NCEP) reanalysis (Kalnay et al. 1996) to aid in

the analysis and identification of physical mechanisms of the coupled modes identified by SVD analysis. To ensure that the results are robust and not affected by one major episode, we have carried out identical SVD analysis for both the 20-year period and for the 19-year period (excluding 1998). Since the statistical results are nearly identical with or without 1998 data, we only show results for those for the full period.

3. Rainfall and SST anomalies during 1997 –98

We start first with the observed monthly rainfall and SST anomalies over ASM domain for JJA 1997 and 1998 (Figs. 1a and b). In both years, the rainfall patterns are quite complex with large month-to-month variations. Major rainfall anomaly centers were found mostly either over the open oceans or anchored to oceanic regions adjacent to the land, such as the Bay of Bengal, the South China Sea, and the eastern Arabian Sea, and the southern tip of the India subcontinent. In 1997, there appeared to be some similarities between the June and August large scale rain patterns, with reduced rainfall over the maritime continent and eastern Indian Ocean. The coastal region of southern China showed above normal rainfall for all three months consistent with the record widespread flood over that region (National Climate Center Report, 1998, private communication). In July and August 1997, below normal SST was found in the Indonesian seas and the eastern equatorial Indian Ocean. A slightly warmer Indian Ocean was noted. However, the overall SST pattern in the ASM region was not very well-organized, with most SST anomalies less than 0.5° C, except for pockets of warm water (0.5 –1° C) in the western Indian Ocean, off the coast of eastern Africa. In 1998, the rainfall patterns had more month-to-month persistence with reduced rainfall over the South China Sea and the far western Pacific and increased rainfall over the central and eastern equatorial Indian Ocean region for all three months. The disastrous flood over the Yangtze River region can be identified with a band of

enhanced rainfall stretching from southwestern China to the south of Japan during June to July. By August, the rainband had shifted northward into northeast China and southern Korea. On the broad scale, the rainfall pattern showed a general eastward shift of the region of reduced rainfall, which resulted in reversal of rainfall anomalies over many sub-regions from those of 1997. The Indian Ocean was uniformly warmer in June 1998. By July and August 1998, the warm water had shifted to the oceanic areas within the maritime continent, while the western and central Indian Ocean SST was below normal, representing a general reversal of the 1997 patterns.

As a background to understand observed monsoon rainfall/SST relationship in the subsequent analyses, we examine the evolutions of basin-scale SST and rainfall for the 20-year period leading up to the 1997-98 El Niño. Figures 2a and b show the time-longitude sections of monthly rainfall and SST anomalies from January 1979 – December 1998. In the SST plot (Fig. 2b), the signatures of the El Niño (1982-83, 1987-88, 1991-92 and 1997-98) and La Niña (1984-85, 1988-89, and 1998-99) were very pronounced. During an El Niño, large positive SST was found stretching from the coastal region of South America to the dateline, and lasting for about a year, typically peaking near October – December. Notice that a well- defined La Niña was developed in late 1998 and 1988 immediately following an El Niño in the previous year. In contrast, from 1984 through 1986 (after the 1982-83 El Niño), and from 1994 through 1995 (after the 1991-92 El Niño), a weak cold phase appeared to linger. Also noted in Fig. 2b was the exceptional warmth of the Indian Ocean and the establishment of strong east-west gradient between the eastern and western Indian Ocean during the latter part of 1997 and early part of 1998 (Yu and Reinecker 1999, Webster et al 1999).

Coherent with the development of the peak phase of El Niño, was the establishment of an east-west dipole rainfall anomalies between the central /eastern Pacific, and the maritime

continent (Fig.2a). This rainfall pattern was associated with the well-known eastward shift of the Walker circulation associated with an El Niño and was most pronounced during the 1982-83 and 1997-98 events. During these two events, enhanced rainfall over the Indian Ocean was also noted. While coherent variations in rainfall and SST anomalies can be identified on the Pacific basin scale, there were strong intraseasonal oscillations in rainfall (Fig. 2a), and to a lesser extent in SST (Fig. 2b) in the ASM sector. This intraseasonal oscillations appeared as somewhat discontinuous, eastward propagating signals originating from the far western India Ocean and terminating near the datelines, except during an El Niño, when they could reach the far eastern Pacific. During summer of 1997, an east-west rainfall dipole developed along the equatorial Indian Ocean at the same time when the aforementioned Indian Ocean east-west SST gradient became well developed. This rainfall-SST dipole continued to develop, reaching a maximum in late 1997 and early 1998. The implication of the dipole precipitation and the east-west SST seesaw on ocean-atmosphere coupling in the Indian Ocean was reported by Webster et al (1999) and Saji et al (1999).

4. Rainfall-SST coupled modes

To identify the dominant modes of coupled rainfall and SST and to elucidate the role of remote vs. regional SST forcings on monsoon rainfall, we have carried out four different sets of SVDs of the monthly rainfall and SST anomaly fields from May through September for the period 1979-1998, using different combinations of global and regional domains. Here, the global domain is defined as the entire tropics and subtropics from 40° S to 40° N, and the ASM domain is defined by the latitude-longitude limits of 20° S–40° N, 30° E –150° E. The four sets of SVDs are:

i) Global SST - Global rainfall (GG)

ii) Global SST - Regional rainfall in the ASM domain (GR)

iii) Remote SST - Regional rainfall in ASM domain (ReR): same as in ii) except that the SST field is now for the global domain minus the ASM domain, and

iv) Regional SST – Regional rainfall in ASM domain (RR)

In the context of this paper, global scale is used generically to mean the domain that covers the entire tropics from 40° S to 40° N. This is to be distinguished from the term basin-scale which will be specifically taken to mean variability that covers the Indo-Pacific basin. The use of different domains for SST and rainfall is an attempt to unravel the intrinsic global rainfall-SST modes (GG), the impact of basin-scale SST on ASM rainfall (GR), the impact of remote SST i.e., outside of the ASM region, on ASM rainfall (ReR) and finally the structure of dominant regional modes from a regional SST and rainfall analysis (RR). It is pointed out that because in reality, regional and global modes are invariably coupled, even the global modes (GG) will reveals aspects of regional characteristics. Likewise, the regional analysis (RR) will be influenced by the global modes. Intrinsic basin-scale modes will be identified by their approximately invariance among the four SVD analysis. In the course of the analysis, we find an interesting linear trend in the SST and rainfall data. However, since the main focus of this work is on interannual variability, we decide to only to point out this in the GG analysis, but defer detailed discussion of the trend, pending further analysis in a separate report. We have verified that the trend does not affect the qualitative description of the modes. However, in order to remove any (slight) effect that the trend may have on the quantitative attributions of observed rainfall in Section 5, we elect to first detrend the data, except in GG, before the SVD analysis is

applied. Since the first two SVD modes are broadly similar in all four analysis, we shall only show the results for GG and GR for descriptions regarding these two modes. For the regional mode, we use the results from GG and RR for comparison.

a. The Global SST - Global Rainfall (GG) Analysis

i) SVD1

The first SVD mode (SVD1) is nearly invariant with respect to the choice of domains and represents truly basin scale variability in global rainfall and SST. The squared covariance percentages explained by this mode in GG is predominant, varying from 53% to 36% (see Table 1) among the various analyses. In all the subsequent discussions, the signs of the anomalies are taken as shown in the figure. The actual sign of the anomalies is dependent on the sign of the corresponding principal component (PC). In this mode, the rainfall pattern is dominated by a large scale, east-west dipole with positive anomaly in the central equatorial Pacific and negative anomaly over the maritime continent (Fig. 3a). In the ASM region, negative rainfall anomalies centers are found over the equatorial eastern Indian Ocean, the South China Sea, and the southern Bay of Bengal, while positive centers are located over the northern Bay of Bengal, southern China, the western Indian Ocean and western Australia. Other features in the global rain field include a tightly coupled north-south dipole in the eastern Pacific, indicating a southward shift of the Intertropical Convergence Zone (ITCZ), and a negative rainfall center over northeastern Brazil. The range of the rainfall anomalies are of the order of -5 to 8 mm/day.

The above rainfall pattern is coupled to a basin scale SST field that is characteristics of the mature phase of El Niño, having a wedge-shaped warm eastern Pacific, a cold western Pacific and eastern Indian Ocean, with cold central subtropical western Pacific in both hemispheres (Fig.

3b) in the form of a horse-shoe. The El Niño related SST pattern in the Indian Ocean features above-normal SST in the western India Ocean, with an east-west SST gradient opposite to that over the Pacific. The warmer water off the coast of East Africa may be an indication of the reduced upwelling associated with a weakened broad-scale monsoon during an El Niño. The PCs of SVD1 for rainfall and SST (Fig. 3c) have an exceedingly high correlation coefficient (cc) of 0.94, showing good correpondence to El Niño and La Niña. This pattern is very similar, but not identical to the first emipirical orthogonal mode using SST alone (not shown). Rather, the PCs are more distinguished by their sharp reversals during the consecutive years of 1983 and 1984, 1987 and 1988, and 1997 and 1998 respectively. What the PCs capture is not so much El Niño or La Niña events by themselves, but rather the phase transition between them in two consecutive years , i.e. the biennial cycle. Because of the switch in polarity of the spatial pattern, SVD1 may be interpreted as the symmetric or mirror-image component of the biennial variability associated with monsoon-ENSO interaction. The biennial tendency and specific role of ASM rainfall in SVD1will be discussed in more detail in later sections.

ii) SVD2

The second SVD mode (SVD2) from GG (Fig. 4) accounts for 16% of the squared co-variance of the global rainfall and SST variability and is well separated from the higher modes (see Table 1). This mode is characterized by a reduction in the positive rainfall anomaly over the central equatorial Pacific (for positive sign of PC2), concomitant with an eastward shift of the reduced-rainfall or drought zone from the maritime continent (as shown in SVD1 in Fig. 3a) to the western Pacific (Fig. 4a). The drought zone extends further eastward in two arms to the eastern Pacific and the South Pacific Convergence Zone (SPCZ). As a result of the shift, much of the Asian monsoon region, including the Indian Ocean and maritime continent, East Asia and

Japan and Australia experienced enhanced rainfall. The SVD2 rainfall pattern is coupled to an emerging cold tongue in the equatorial central Pacific, a shrinking warm water region in the eastern Pacific and an expanding warm pool in the vicinity of the maritime continent (Fig. 4b). In contrast to SVD1, the rainfall PC show only weak biennial transitions, but rather episodic variations with strong positive projections in 1998, 1988 and 1983. The signal is very pronounced and coherent from month to month, during 1998 and 1983. The positive swings are also quite evident in the SST PC for SVD2, which is quite well correlated with the rainfall PC (cc=0.79). The negative swings are generally smaller. This may reflect an inherent asymmetry in the growth and decay of an El Niño and/or the development of a La Niña. Further evidence provided in later sections suggest that SVD2 may be considered as a mixed mode, in that it possesses strong regional as well as basin-scale characteristics.

(iii) SVD3

The third SVD mode (SVD3) for GG explains about 7% of the squared covariance, and is still well separated from the higher SVDs based on the criterion of North et al (1972). The rainfall pattern (Fig. 5a) appears to be quite regional, featuring a dipole across the western Indian Ocean/Bay of Bengal and eastern Indian Ocean/maritime continent. Also found is a secondary rainfall dipole between the oceanic region surrounding central America, and the land region of northern South American. This rainfall pattern is coupled to a SST distribution that depicts an overall, broad scale tropical warming, except near coastal region of northern South America and the coastal regions of the Asian and African land masses (Fig. 5b). The correlation between the two PCs in Fig. 5c is quite high (cc=0.85), indicating that this is a highly coupled mode, even though its share of total covariance is small compared to SVD1 and SVD2. The SST pattern shows rather pronounced warming over the southeastern Indian Ocean and the central tropical

and subtropical Pacific. A large area of cooling is found over the North Pacific. The magnitude of the warming is of the order of 0.1-0.5° C, considerably smaller than those associated with the fluctuation of SVD1 and SVD 2 (order of 1-3^0 C). The aforementioned spatial and temporal patterns suggest that the global SVD3 pertains to a global warming signal which is tampered by local air-sea interactions in the Asian as well as the South American regions, at both end of the Indo-Pacific basin. As noted earlier, discussion on the implication of possible effect of the trend is out of the scope of this work.

b. The Global SST-Regional Rainfall (GR) analysis

The GR analysis targets the rainfall variability in the ASM region and its relationship with global SST. As explained before, the rainfall and SST patterns for SVD1 and SVD2 are qualitatively similar among all the SVD analysis with different domains, demonstrating that these are mostly basin scale modes. Based on the GR analysis, additional features arising from interaction of ASM rainfall may be identified. Since the SVD1 and SVD2 modes are already introduced in the global analysis GG, the discussion in this section will focus on the physical interpretation and additional information gained from examining SVD1 and SVD2 based on GR.

i) SVD1: the basin-scale mode

In the GR analysis, the squared covariance explained by SVD1 is 47%, slightly less than that for GG. The SST pattern of SVD1 in GR (Fig. 6c) and its PC (Fig.6b) are virtually identical to that in GG (Figs. 3b and c), affirming that this is a truly basin-scale mode. The rainfall pattern (Fig. 6a) and its corresponding PCs for SVD1 (Fig. 6b) is essentially the same as that in GG, except that the spatial features are more sharply defined and the temporal fluctuations have larger amplitude and more month-to-month variability. Negative rainfall anomalies (in the sense of the PC shown in Fig. 6b) are found over the oceanic regions of eastern Indian Ocean,

Indonesia, South China Sea and the subtropical western Pacific. These negative anomalies are surrounded by somewhat isolated sub-regional scale positive rainfall anomalies located over the Bay of Bengal, southern China and the western Indian Ocean. By and large, the monthly anomalies tend to have the same sign within the same year, and the rainfall PC is highly correlated with the corresponding SST time variation (cc = 0.78). The aforementioned biennial switches occurring in 1983-84, 1987-88 and 1997-98 are quite obvious in both PCs.

Figure 6d shows the regression of the 850 hPa wind vectors (plotted as streamlines, with regions having correlation exceeding 95% significance shaded) against the rainfall PC. The appearance of a double anticyclone over the Indian Ocean is dynamically consistent with the large scale negative rainfall anomalies show in Fig. 6a. This implies reduced atmospheric latent heating accompanied by descending motion over the eastern equatorial Indian Ocean/maritime continent induced by the anomalous Walker circulation. The northerly wind flow over the western Indian Ocean is indicative of a weakening of the large scale ASM. The signature of the anomalous Walker circulation is very clear in the regressed 200hPa wind field (Fig. 6e), showing strong upper level anticyclones straddling easterlies over the equatorial western/central Pacific, and confluence (sinking motion) over the maritime continent. As evident in the extensive region of upper level westerlies over the Indian Ocean and the anomalous cyclonic circulation over Tibet, the large scale ASM is strongly reduced in 1992, 1987 and 1997 (positive PCs in Fig. 6b), and enhanced in 1984, 1988 and 1998 (negative PCs in Fig. 6b) . It is likely that the enhanced precipitation (rising motion) in the monsoon land regions may be connected to the reduced precipitation (descending motion) in the equatorial Indian Ocean through an anomalous local Hadley circulation. The strong low-level anomalous westerly wind across the Pacific, and the upper level westerlies over the Indian Ocean and easterlies over the Pacific provide strong

evidence of the basin-scale nature of this mode. The shift in the Walker circulation and the possible induced changes in the local Hadley circulation as reflected in SVD1, may be considered as the first –order or direct impact of El Niño -La Niña on the ASM associated with the transition between the warm and cold phases.

It should be pointed out that while the SVD1 mode captures the basic ENSO-monsoon coupling , it is not identical to the El Niño or La Niña mode itself. An EOF analysis of basin-scale SST itself (not shown) yields a quasi- four year cycle without the pronounced 2-year switch between the warm and cold phase that characterizes SVD1. As stated before, physically, SVD1 describes the symmetric switch in polarity or mirror image aspect of the basin scale monsoon-SST warm-cold cycle. As discussed previously, the switch in polarity of the warm and cold events is apparent also in Fig. 2a. However, as noted in the discussion of Fig. 2a, El Niño and La Niña are not simply mirror images of each other. This brings us to the second mode.

ii) SVD2: the mixed mode:

The SVD2 in GR can be identified broadly with that in GG, as can be seen in the almost identical global SST pattern in the Pacific region between GR (Fig. 7c) and GG (Fig. 4b). There may be some slight differences in the SST pattern in the Indian Ocean due to local air-sea interactions. More revealing is in the ASM rainfall pattern and its PCs from GR (Figs. 7a and b) Here, the rainfall features zonally oriented alternating broad dry and wet belts, with embedding sub-regional features, broadly resembling those shown in Fig 4a. The sub-regional features include positive rainfall anomalies over the Yangtze River Basin and southern Japan (~30° N), the Bay of Bengal, and the eastern Arabian Sea; negative anomalies over the western Pacific and South China Seas, and positive anomalies anchored by the maritime continent, and an ITCZ-like structure stretching across the Indian ocean between the equator and 15°S. The rainfall PC

shows pronounced month-to-month variability (Fig. 7b). During MJJAS of 1998 and 1983, the rainfall and SST PCs have strong positive projections and high degree of coherence. The complex sub-regional scale features, and the pronounced month-to-month variability suggest that this mode is strongly impacted by subseasonal scale variability, possibly associated with the intraseasonal oscillations, as discussed in Fig. 2. The regressed 850 hPa wind pattern (Fig. 7d) indicates the rainfall variability of this mode is linked to a strong low level anticyclone over the subtropical western Pacific, just off the coast of East Asia. During its positive phase (developing La Niña), the western Pacific anticyclone (WPA) induces strong easterlies in the equatorial regions of the western Pacific, across the South China Sea into the Bay of Bengal. The WPA has been shown to be instrumental in leading to excessive rainfall over the Yangtze River region as occurred in 1998, by transporting moisture from the South China Sea into the region (Lau and Weng 2000). Additionally, the WPA appears to be connected to basin-scale anomalous easterly wind emanating from the southeastern Pacific. The regressed 200 hPa (Fig. 7e) wind shows that the WPA is associated with an upper level wave pattern in the region of the subtropical East Asian jet, comprising a ridge over coastal East Asia and an upper level low over the subtropical central Pacific. In the equatorial region of the eastern Indian Ocean, maritime continent and western Pacific, SVD2 (in its positive phase) is associated with upper level westerlies and southwesterlies, reversed from the low level flow. The large scale circulation patterns are similar to those observed for the intraseasonal oscillations in the ASM region (Knutson and Weickman 1987, and Rui and Wang 1990). These patterns also suggest a weakening of the large scale ASM monsoon during the positive phase of SVD2, most pronounced in 1998, 1987 and 1983 (Fig. 7b). As mentioned previously, and evident in the associated SST pattern (Fig. 7c) and its correpsonding PC (Fig. 7b), this mode may signify the asymmetric, or non-mirror image

component of the transition phase of El Niño /La Niña. The coupling of the rainfall and SST PCs are only moderate (cc=0.59). The lower correlation is probably due to the strong subseasonal scale regional variability inherent in this mode. Due to the presence of both pronounced regional and basin-wide signatures, this mode may arise from the interaction of monsoon and basin-scale SST, as well as regional coupled SST processes. The impacts of El Niño on this mode are likely to be "indirect", i.e., though enhancement of local processes and/or modification of the El Niño by the monsoon itself. These impacts are probably nonlinear in character. Henceforth we shall refer to SVD2 as the mixed mode.

c. Regional SST-Regional Rainfall Analysis (RR)

In this subsection, we focus on the discussion of the regional mode SVD3 based on RR. Here, the regional mode accounts for approximately 8% of the squared covariance, somewhat larger than those (5-7 %) based on the other analyses (see Table 1). This amount is still relatively small compared to the two dominant modes, SVD1 and SVD2. As noted before, this mode is also affected by a linear trend, which has been removed for this analysis. It is only marginally separated from the higher modes. Hence the results here must be taken with caution. The rainfall pattern for this mode is characterized by an east-west rainfall dipole across the equatorial Indian Ocean between equator and 15° S (Fig. 8a). Elsewhere the rainfall anomalies are weak, and appear to form bands oriented northwest to southeast, spanning the eastern Indian Ocean and western Pacific. This orientation appears to bear some relationship with the SST anomalies, which spots a northwest-southeast oriented warm tongue stretching from the southeastern Indian Ocean off the west coast of Australia to the central equatorial Indian Ocean (Fig. 8b). Cold water is found off the west coast of Sumatra in the extreme eastern Indian Ocean and much of the South China Sea and subtropical western Pacific adjacent to the East Asian continent (Fig.

8b). The correlation between the two PCs are quite high (cc=0.70). They exhibit variations of 3-4 years and longer time scales, but bearing little relationship to El Niño (Fig. 8c).

The regressed 850 hPa wind field (Fig. 8d) shows that there is no significant basin-scale wind correlation over the vast stretch of the central and eastern Pacific. Significant wind correlation is confined to the ASM region, with a circulation pattern suggesting low level inter-hemispheric transport originating from an anticyclone over the southeastern Indian Ocean via westerlies across India and IndoChina, ending in a cyclone over the subtropical western Pacific. The pattern appears to be consistent with orientation of SST anomalies in the eastern Indian Ocean for this mode (Fig. 8b). The apparent coupling between the anticyclonic flow in the southern hemisphere to a cyclonic flow in the northern hemisphere is also dynamically consistent with a local Hadley cell connected by heat sources and sinks away from the equator. The 200 hPa regressed wind shows little basin-scale features in the equatorial region, but suggests a connection with the wintertime circulation of the southern hemisphere.

While the details of the rainfall and circulation features may be somewhat questionable due to its marginal significance, the lack of basin-scale wind features supports the interpretation of this mode as a regional mode, unrelated to El Niño /La Niña. Recent findings of similar rainfall dipole in the Indian Ocean by Webster et al (1999) and Saji et al (1999) may provide some indirect support that this mode may be physical. These authors find that the modes are most prominent in September –November. This may be one of the reasons for the weak signal of this regional mode noted in this analysis

5. Reconstruction and attribution of ASM rainfall anomalies

Having identified the principal coupled rainfall-SST modes and their possible physical underpinnings, we now proceed to evaluate the possible causes of the observed interannual ASM

rainfall anomalies. Using the procedure as described in Lau and Wu (1999), we compute the cumulative anomalous correlation (CAC), defined by

$$CAC_{i,j} = < O_j, \sum_{k=1}^{i} SVD(k) * PC(k)_j >,$$

Where, j is the year index; < > denotes the normalized pattern correlation over a chosen domain between the observed rainfall, Oj, and the reconstructed rainfall pattern using up to the ith SVD vector. The incremental contribution to the anomaly correlation by each mode is given by $A_{1j} = CAC_{1,j}$, $A_{2,j} = CAC_{2,j} - CAC_{1,j}$ etc. Since the CAC is a measure of the similarity of the re-constructed rainfall field to the observed with perfect knowledge of the SST field, it can also be considered as an upper bound on the predictability of the ASM rainfall. Based on the explained co-variance, it is likely that a major portion of the predictability may reside in the first two SVD modes and to a lesser degree also in SVD3. Inspection of the mode-by-mode contribution to the reconstructed rainfall field (not shown) indicates that SVD4 and SVD5 may contribute to realistic sub-regional features that significantly increase the CAC and therefore may enhance predictability in some years. However, the higher order (>5) modes are increasingly variable, containing small scale features that are unlikely to have any predictability. This is also evident in the fact that the contribution to the CAC in most cases levels off after the 4th and the 5th SVD modes. Therefore, we will consider the CAC's only up to the 5th SVD mode as the upper bound to predictability in the following discussions. Using the aforementioned procedure, we have computed the attributions of the all- ASM domain as well as various monsoon subdomains. They will be discussed separately.

a. All- ASM domain

Fig. 9a shows the CAC for up to the 5th SVD mode each year for the entire data period for the entire ASM domain for GR. The contribution of each mode to the observed rainfall

variability is shown by the length of the vertical bars, with different shadings for each mode. The direct impact of the basin-scale SST anomalies (SVD1) is not very high (CAC< 0.25). When the mixed mode (SVD2) is included, the CAC increases substantially (> 0.3). For all years, the contribution of the regional modes (SVD 3 to 5) to the CAC is non-negligible. Indeed, to achieve useful "prediction" skill, say, CAC value of 0.5 or higher, the contribution of the regional modes are required, except in years of strong La Niña, i.e., 1998 and 1984, when the first two modes suffice. It is noticed that the basin-scale contributions from SVD1 and/or SVD2 are generally larger in the developing phase of La Niña (1998, 1988, 1984) compared to the developing El Niño (1982, 1987, 1997). Since the regional effects are partially represented by SVD2, and by SVD3 and higher modes, they contribute as large as, and sometimes larger than basin-scale effects.

Fig. 9b shows the CAC for ReR, in which the SVD modes are computed from ASM rainfall and SST from outside the ASM region. With the SST information in the ASM region withheld, the total CAC (up to the 5th mode) for all years are generally lower than GR (Fig. 9a). The reduction is mostly due to the reduced contributions from SVD3 and/or higher order modes. The contribution by SVD1 remains about the same and that by SVD2 is generally smaller. Notice that the contributions of SVD1 and SVD2 remain very high and almost unchanged from GR in 1998, suggesting that remote forcing dominate rainfall variability over the ASM region for that year. These results are consistent with the physical interpretations that SVD1 is a basin-scale mode, and therefore can be adequately represented by remote SST variations in ReR. On the other hand, SVD3 and higher modes, and SVD2 partially, involve coupled SST processes in the ASM region and therefore are not as well represented in ReR.

To further illustrate the impact of remote vs. regional SST forcings on ASM rainfall, we have computed the year-by-year error variance of the reconstructed rainfall anomalies relative to the observed over the ASM region for the three cases, GR, ReR and RR (Fig. 10). It is obvious that ASM rainfall anomalies "predicted" based only on remote SSTA forcing (ReR) has the largest error variance. The inclusion of SST information in the ASM region in GR and RR can substantially reduce the error variance by 20-30 %. In individual years, the reduction can be higher or less. For example, in 1997, the error variance is reduced over 40% from about 3 .1 to 1.7 $(mm/day)^2$. In contrast, in 1998, the error reduction due to inclusion of regional processes is considerably less. This is consistent with the results shown in Fig. 9, which indicates that the basin-scale impacts of El Niño /La Niña is very large in 1998. Note that the use of global SST (GR) produces only a slight reduction in the error variance compared to the use of SST in the ASM region only (RR). This is because the SST in the ASM region is affected by basin-scale as well as regional scale processes. Hence, SST variability in the ASM region contains basically most, if not all, the regional and basin-scale information needed to predict ASM rainfall. However, this is not to say that that we do not need remote SST anomaly for monsoon prediction. In fact, prediction of SSTA in the central and eastern Pacific has much better skill compared those in the ASM region. We also note that in 1986, the error variance is very small for all three cases. An inspection of the monthly rainfall patterns over the ASM indicates that the 1986 anomalies are very mild and have very little month-to-month variability, so that much of variability (including magnitude) is captured by the basin-scale SST fluctuation.

b. ASM subdomains

In this subsection, we provide quantitative estimates of attributions to rainfall anomalies for two key subdomains of the ASM, i.e., the South Asian monsoon (SAM) (70-100° E, 10-30° N)

including the Bay of Bengal, and the East Asian monsoon (EAM) (100-140° E, 10-35° N). They are shown as outlined boxes in Fig. 1. Lau et al (2000) have shown that these two subdomains possess fundamentally different dynamics and should be examined separately for monsoon-ENSO interactions. Here, we will focus only on the comparison between the years, 1982-84, and 1997-98 which cover the warm-to-cold phase transition period for the two major El Niño of the 20th century.

i) The SAM subdomain

The CAC of the GR SVD modes for the South Asian monsoon (SAM) subdomain are shown in Table 2. As noted in the discussion of Fig. 2, the 1982-83 El Niño differs from the 1997-98 event in that the biennial switch, i.e., the cold phase transition, is not as well developed with the warm phase lingered on through the end of 1983 and the cold phase through 1984-85. This is reflected in its impact on SAM as shown in Table 2. First, we consider the similarities between the two events. During the growth phase of the warm events, 1982 and 1997, the basin-scale effects, both direct and indirect (SVD1 and SVD2) are small or non-existent, as indicated by the CAC of 0.04 and 0.0 for SVD1-2 for 1982 and 1997 respectively. In these two years, most of the rainfall anomalies over this subdomain are mostly due to regional scale processes (SVD3 and higher). During the developing cold phase (1983, 1984 and1998), the basin-scale influences from SVD1 and SVD2 are increased substantially, as indicated by the large CAC (=.39, .58, and .57) compared to the mean (=.32). A feature common to both events is that the basin scale impact (SVD1 and SVD2) on SAM is strongest in the summer season (1998, 1984) preceding the peak cold SST which occurs 1-2 seasons later (see also discussion in Section 6). A key difference between the two events, is that in 1983 and 1984, there are no changes in the CAC between SVD1 and SVD1-2. This means that there is little or no influence

from the mixed mode (which include intraseasonal variability and basin-scale SST effects), while the effect of this mode is very pronounced in 1998. If we assume that potential predictabilty of the ASM comes mostly from the basin-scale and mixed modes, then we see substantial increase in potential predictability of SAM in 1984 and 1998 with CAC reaching 0.70 and 0.74, respectively compared to the mean of 0.50. During the warm phase of 1982 and 1997, the impact of basin-scale SST on SAM is almost non-existent, even though for the ASM domain as whole, there are significant basin scale impacts (see discussion for Fig. 9). This illustrates the important point that subregional scale variability is generally not representative of the entire ASM region.

We note also from comparing SVD1 to SVD1-2 over the 20-year mean that in general, SVD1 (the direct ENSO impact), contributes considerably more than SVD2 to the CAC over the SAM domain (0.28 for SVD1 out of the total of 0.32 for both) over the SAM domain. Physically, this means that for interannual variability, SAM is affected more strongly by the shift in the Walker circulation than by the WPA and associated intraseasonal oscillations.

ii) The EAM subdomain

Table 3 shows the CAC for the EAM subdomain. In the developing warm phase, 1982 and 1997, the contributions from basin-scale effects (SVD1 and 2) are small (=0.28 and 0.23 respectively) and significantly below the 20-year mean (=0.36). However the regional contributions (SVD 3 and higher) seem to increase. As a result, the total CAC (SVD1-5) for the two years , 0.39 and 0.44 respectively are not significantly different from the 20-year mean of 0.42. During the decaying warm phase (1983), or developing cold phase (1984, 1998), the contributions from SVD1 and/or SVD2 more than double, indicating large increase in basin-scale and related regional SST influences. This increase, together with additional contributions

from the regional modes (SVD3 and higher) boost the total CAC to above 0.70 for 1983, 1984 and 1998, well above the 20-year mean (=0.42). Note that for 1998, there is no contribution from SVD1, and that the mixed mode (SVD2) contributes nearly almost all the CAC. This implies the strong influence of the WPA on the EAM during that year. Again, we note that it is in the decaying warm phase, or the developing cold phase that the monsoon-ENSO connection seems to be sharply enhanced.

The break-down for the 20-year mean contribution indicates that the basin-scale mode (SVD1) and the mixed mode (SVD2) both influence the EAM region, with stronger influence from the latter. In other words, the EAM is more strongly impacted by SST forcings via the WPA, and less so from the direct impact from the shift of the Walker circulation. Since the WPA effect is "indirect", arising form the interaction of intraseasonal variability and basin-scale forcings, it is less predictable and may be the reason for a lack of a robust ENSO signal in EAM (cf., Lau et al. 2000).

6. A hypothesis

In previous sections, we have found that the evolution of the El Niño /La Niña cycles during 1982-84 and the 1997-98 are quite different and that their impacts on the ASM and its subdomains are also different. In particular, we have noted the year in which the transition form warm-to-cold phase appears to show the stronger monsoon-ENSO connection. Here, we address the converse problem and explore the hypothesis that the 1982-84 and the 1997-98 El Niño /La Niña evolved differently *because* the forcings by the ASM on the El Niño's were different. As discussed in Section 5, SVD1 is associated with anomalous low level westerlies (easterlies) in the equatorial western Pacific resulting from the eastward (westward) shift of the Walker circulation during an El Niño (La Niña). Likewise, the mixed mode (SVD2) is

associated, during a La Niña, with low level easterlies in the equatorial western Pacific, linked to the WPA off the east coast of East Asia. In the following, we shall use these identifications in examining the possible effects of these ASM related wind forcings on the evolution of El Niño /La Niña.

Fig. 11 shows the Niño -3.4 SST variation, and the rainfall PCs, which represent the strength and sign of the SVD1 and SVD2 modes for the periods 1981 –84, 1986-1989 and 1996-1998, including the warm and cold phases transitions. To facilitate the comparison, the sign of the PC for SVD2 has been reversed, so that a positive (negative) sign in both PCs denotes anomalous westerlies (easterlies) in the equatorial western Pacific. To focus attention, the following discussion will be devoted mostly to the two major events, 1982-84 and 1997-98. Comments on the 1987-89 will be provided when appropriate. As noted in the discussion of Fig. 2b and from the Niño -3.4 SST time series (Fig. 11a), the 1982-83 event had a longer cycle, with the cold and warm phases lasting about 4 years, while the 1997-98 events had a much shorter cycle of approximately two years (Fig. 11c). During JJA 1982, SVD1 was large and positive, indicating prevailing low level westerly wind over the Pacific from the eastward shift of the Walker circulation (see Fig. 6d). This westerly wind increase was likely to excite eastward propagating oceanic Kelvin waves, and contribute to the development of the warm phase (Kessler et al., 1996). Since SVD2 was weak, the WPA contributed very little to the warming in JJA 1982. As the Niño 3.4 SST evolved, it peaked around October –December, 1982. The turn-around may have to do with various mechanisms, including possible interactions with the winter monsoon which will not be discussed here. In the following summer, SVD2, via the WPA, contributed strong low level easterlies over the western Pacific. This easterly wind was, however, opposed by westerly wind remaining from the warm event, i.e., the Walker circulation remained shifted

eastward from its climatological position, resulting only in a weak cold event in 1984. During JJA 1984, strong contribution from SVD1 and partially from SVD2 produced easterly wind over the western Pacific, leading to the further development of La Niña in the winter of 1984-85.

Fig. 11c shows that the growth phase of the 1997-98 El Niño was similar to that of 1982-83, in that SVD1, i.e., eastward shift of the Walker circulation, was mostly responsible for the rapid warming. Similar to 1982, the Niño -3.4 SST reached its peaked in October-December, 1997. However, the decay phase of El Niño evolved very differently. From May through September, 1998, both SVD1 (the Walker circulation) and SVD2 (the WPA) were strong and extremely coherent. They conspired to produce very strong easterly wind anomalies over the western Pacific. As a result, the El Niño rapidly terminated and La Niña emerge within 12-months, giving rise to a very distinct biennial signal. The aforementioned interplay between the Walker circulation and the WPA, in relation to Niño 3.4 SST variation appeared to also fit the 1987-88 event (Fig. 11b), which was similar to the 1997-98 event in having a distinct biennial signal. Hence it is plausible that, not only the El Niño impacts the ASM, but wind anomalies derived from ASM anomalies may have a strong impact on the evolution of El Niño /La Niña cycle.

7. Conclusions

Using 20-years of rainfall and SST data, we have identified natural modes variability in the Asian monsoon region and explore their physical underpinnings. Using these natural modes, we assess the role of monsoon-ENSO coupling and other physical processes in contributing to rainfall variability over the all- Asia monsoon domain, as well as the South Asia and the East Asian subdomains. Based on the present results, we propose a plausible mechanism by which the ASM may affect the evolution of ENSO.

We found three natural, recurring coupled modes that may play important roles in interannual variability of the ASM rainfall. The most dominant coupled mode accounts for 36-53% of the covariance, depending on the analysis domain. It is characterized by a basin-wide coherent pattern, associated with the east-west shifts of the Walker circulation and SST anomaly patterns across the equatorial Indo-Pacific basin that occur during the transition phases of El Niño and La Niña. In this mode, the ASM rainfall is affected by large scale sinking (rising) motions over the equatorial Indian Ocean and maritime continent, and induced changes in the local Hadley overturnings. This coupled mode differs from the traditional ENSO SST mode, in that it emphasizes the symmetric or mirror-image component of the transition, with a strong biennial tendency. This mode may be considered as the first order or direct impact of ENSO on the ASM.

The second mode is a mixed basin scale and regional coupled mode with large month-to-month variability suggestive of strong influence by intraseasonal oscillations. It accounts for approximately 16 –22 % of the total covariance, depending on the size of the domains. This mode is characterized by strong anomalous anticyclone in the subtropical western Pacific, off the coast of East Asia, coupled to a developing anomalous warm pool in the oceanic regions adjacent to the ASM land masses, i.e., the eastern Indian Ocean, the South China Sea and the western Pacific, and to an emerging cold tongue in the equatorial central Pacific. This mode appears to describe the asymmetric or the non-mirror image component associated with El Niño /La Niña transition. During 1998, this mode had very strong influence on rainfall anomalies over East Asia region. This mode may be construed as providing the "indrect" impact of ENSO on monsoon in that it is governed by regional monsoon coupled processes and interactions with basin-scale SST and winds

The third mode which accounts up to 8% of the rainfall/SST covariability, consists of a rainfall dipole in the Indian Ocean just south of the equator, coupled to a northwest-southeast oriented SST anomaly in the Southern Indian Ocean. This mode exhibits features that are suggestive of regional interhemispheric teleonnections between the Australian wintertime circulation and the ASM.

An analyses based on cumulative anomaly correlation shows that for the all-ASM domain, regional modes play an important role, in addition to basin-scale or ENSO-related modes in determining ASM rainfall variability. Different sub-regions within the ASM may be impacted differently by the various natural modes. For example, the South Asian monsoon rainfall is affected more by the east-west shift in Walker circulation, while the East Asian monsoon more by the West Pacific Anticyclone. Monsoon-ENSO connection appears to possess an intrinsic asymmetry, being stronger during the summer preceding a well-defined La Niña, i.e., 1984, 1988, 1998, and less pronounced during the developing warm phase, 1982, 1987 and 1997. All three modes may contribute to the potential predictability of the ASM.

Our results suggest that strong monsoon-ENSO tend to occur with a pronounced 2-year polarity switch in basin scale SST anomalies, i.e., the transition phases, so that monsoon-ENSO relationship need to be considered in pairs of years, in relationship to the evolution of SST. Based on the present results, we have articulated a possible mechanism in which the ASM may induce a strong biennial signal, modulating ENSO cycles. We argue that in addition to the well-know eastward shift of the Walker circulation associated with El Niño /La Niña transition, the western Pacific anticyclone may be a crucial link that determines how biennial and intraseasonal oscillations may influence monsoon-ENSO interactions. The full interaction of

monsoon and the ENSO cycles, however, is likely to involve both the winter and summer components of the Asian-Australian monsoon.

Acknowledgment

This work is supported jointly by the NASA Global Modeling and Data Analysis Program, and the TRMM project.

Reference

Ailikun, B. and T. Yasunari, 1999: On the two indices of Asian summer monsoon variability and their implications. Part I: the composite of two indices in summer. *J. Meteor. Soc. Japan* (submitted).

Chandrasekar, A. and A. Kitoh, 1999: Impact of localized sea surface temperature anomalies over the equatorial Indian Ocean on the Indian summer monsoon. *J. Metoer. Soc. Japan*, **76**, 841-853.

Goswami, B. N., V. Krinshamurthy and H. Annamalai, 1999: A broad scale circulation index for the interannual variability of the Indian summer monsoon. *Quart. J. Roy. Meteor. Soc.*, **125**, 611-634.

Goswami, B. N., D. Sengputa and G. Sureshkumar, 1998: Intraseasonal oscillations and interannual variability of surface winds over the Indian monsoon region. *Proc. Ind. Acad. Sci, (Earth Planet Sci.)*, **107**, 45-64.

Ju, J. and J. Slingo, 1995: The Asian summer monsoon and ENSO. *Quart. J. roy Meteor. Soc.*, **121**, 1133-1168.

Kalnay, E., M. Kanamitsu, R. Kistler, W. Collins, D. Deaven, L. Gandin, M. Iredell, S. Saha, G. White, J. Woollen, Y. Zhu, M. Chelliah, W. Ebisuzaki, W. Higgins, J. Janowiak, K. C. Mo, C. Ropelewski, J. Wang, A. Leetmaa, R. Reynolds, Roy Jenne and Dennis Joseph, 1996: The NCEP/NCAR 40-year reanalysis Project. *Bull. Am. Meteor. Soc.*, **77**, 437-471.

Kessler, W. S., M. J. McPhaden and K. M. Weickmann, 1996: Forcing of intraseasonal Kelvin waves in the equatorial Pacific. *J. Geophys. Res.*, **100**, 10613-10631.

Knutson,, T., and K. M. Weickmann, 1987: 30-60 day atmospheric oscillations: Composite life cycles of convection and circulation anomalies. *Mon. Wea. Rev.*, **115**, 1407-1436.

Lau, K. -M. and S. Yang, 1996: The Asian monsoon and the predictability of the tropical ocean-atmosphere system. *Quart. J. Royal. Met. Soc.*, **122,** 945-957.

Lau, K. M., H. T. Wu, 1999: An Assessment of the Impact of the 1997-98 El Niño on the Asian-Austrialian Monsoon. *Geophys. Res. Lett.*, **26**, 1747-1750.

Lau, K. M., K. M. Kim, and S. Yang, 2000: Internal Dynamics and Boundary Forcing Characteristics Associated with Interannual Variability of the Asian Summer Monsoon. *J. Climate*, **in press.**

Lau, K. M. and H. Weng, 2000: Coherent modes of global SST and summer rainfall over China: an assessment of the regional impacts of the 1997-98 El Niño /La Niña. *J. Climate*. (submitted).

Li, C. and M. Yanai, 1996: The onset and interannual variability of the Asian summer monsoon and relation to land-sea thermal contrast. *J. Climate*, **9**, 358-375.

Meehl, G. A., and J. Arblaster, 1998: The Asian-Australian monsoon and El Niño -Southern Oscillation in the NCAR climate system model. *J. Climate*. **11**, 1357-1387.

Meehl, G. A., 1997: The South Asian monsoon and the tropospheric biennial oscillation. *J. Climate.*, **10**, 1921-1943.

Rasmusson, E. M, and T. H. Carpenter, 1983: The relationship between eastern equatorial Pacific seas surface temperature and rainfall over India and Sri Lanka. *Mon. Wea. Rev.*, **111**, 517-528.

Reynolds, R and T. M. Smith, 1994: Improved global sea surface temperature analysis using optimum interpolation. *J. Climate*, **7**, 929-948.

Rui, H. and B. Wang, 1990: Development characteristics and dynamic structure of tropical intraseasonal convection anomalies. *J. Atmos. Sci.*, 47, 357-379.

Saji, N. H., B. N. Goswami, P. N. Vinayachandran, and T. Yamagata, 1999: A dipole mode in the tropical Indian Ocean. *Nature*, **401**, 360-362.

Shen, X., and M. Kimoto, 1999: Influence of El Niño on the 1997 Indian summer monsoon. *J. Meteor. Soc. Japan,* **77**, 1023-1037.

Shen, S.-H., and K. M. Lau, 1995: Biennial oscillation associated with the East Asian summer monsoon and tropical sea surface temperature . *J. Meteor. Soc. Japan,* **73,** 105-124.

Shukla, J. and D. Paolino, 1983: The Southern Oscillation and the long-range forecasting of monsoon rainfall over India. *Mon. Wea. Rev.,* **111**, 1830-1837.

Wang, B., and Z. Fan, 1999: Choice of South Asian summer monsoon indices. *Bull. Am. Meteor. Soc.*, **80**, 629-638.

Webster, P. J. and S. Yang, 1992: Monsoon and ENSO: Selectively interactive systems.*Quart. J. R. Meteorol. Soc.*, **118**, 877-926.

Webster, P. J., A. Moore, J. Loschnigg, and R. Leban, 1999: Coupled ocean-atmosphere dynamics in the Indian Ocean during 1997-98. *Nature*, **401**, 356-360.

Xie, Pingping and P. A. Arkin, 1997: Global precipitation: a 17-year monthly analysis based on gauge observations, satellite estimates and numerical model outputs. *Bull. Am. Meteor. Soc.* ,**78**, 2539-2558.

Yu, L. and M. M. Rienecker, 1999: Mechanisms for the Indian ocean warming during the 1997-98 El Niño. *Geophys. Res. Lett.,* **26**(6), 735-738.

Table 1 Percentage of squared covariance explained by the first five SVDs of monthly rainfall and SST for MJJAS for various domains, GG, GR, ReR and RR. See text for definitions of the domains.

	SVD1	SVD2	SVD3	SVD4	SVD5
GG	53	16	7	3	3
GR	47	16	5	4	3
ReR	53	15	5	3	3
RR	36	26	8	6	4

Table 2 CAC contribution to the observed South Asia monsoon rainfall anomalies by the coupled modes. Cumulative contributions up to the Nth mode in indicated by SVD1-N. The incremental contribution from each mode can be obtained as the difference with the column to the left.

SAM	SVD1-1	SVD1-2	SVD1-3	SVD 1-5
1982	0.0	0.04	.15	.51
1983	.39	.39	.40	.40
1984	.58	.58	.60	.70
Mean (1979-98)	**.28**	**.32**	**.40**	**.50**
1997	.0	.0	.22	.54
1998	.15	.57	.64	.74

Table 3 Same as in Table 2, except for the East Asia monsoon rainfall

EAM	SVD1-1	SVD1-2	SVD 1-3	SVD 1-5
1982	.17	.28	.33	.39
1983	.38	.62	.70	.70
1984	.40	.67	.70	.71
Mean (1979-98)	**.10**	**.36**	**.38**	**.42**
1997	.2	.23	.34	.44
1998	.0	.62	.67	.70

Figure Captions

Figure 1 Rainfall anomalies (mm/day) and sea surface temperature (° C) during June, July, August of a) 1997 and b) 1998.

Figure 2 Time-longitude sections of a) monthly rainfall anomalies and b) monthly SST anomalies for the period 1979-1998

Figure 3 Singular eigenvector of SVD1 based on GG, for a) rainfall, b) SST and c) the corresponding PCs, as labeled.

Figure 4 Same as in Fig.3, except for SVD2 for GG.

Figure 5 Same as in Fig.3, except for SVD3 for GG.

Figure 6 a) Singular eigenvectors of ASM rainfall for SVD1 based on GR,

b) corresponding PCs for rainfall and SST,

c) singular eigenvectors of global SST for SVD1 based on GR ,

d) streamline based on regression of 850 hPa vectorwind against rainfall PC in b) with regions exceeding 95% significance shaded, and

e) same as in d) except for streamline based on regression of 200 hPa vector winds

Figure 7 Same as in Fig. 6, except for SVD2 for GR.

Figure 8 Singular eigenvector o for SVD3, based on RR for a) rainfall, b) SST , c) corresponding PCs as labeled, and d) regression of 850hPa vector wind against rainfall PC, and e) regression of 200mb hPa wind against rainfall PC.

Figure 9 Year-by-year cumulative anomaly correlation between reconstructed and observed ASM rainfall for a) Global SST and regional rainfall (GR) and b) Remote SST and regional rainfall (ReR) . Red bar denotes contribution by SVD1. Incremental

contributions by SVD2, SVD3, SVD4 plus SVD5 are indicated by blue, green and yellow respectively.

Figure 10 Year-by-year error variance between observed and reconstructed rainfall based on the first five singular vectors for Global SST-Regional Rainfall (GR), Remote SST –Regional Rainfall (ReR) and Regional SST and Regional rainfall (RR).

Figure 11. Time series of Niño -3.4 SST during 1981-84, 1986-89 and 1996-98, showing relationship of SST variation to PCs for SVD1 (dark shaded bar) and SVD2 (light shaded bar). Positive (negative) values denote westerly (easterly) wind anomalies in the western Pacific.

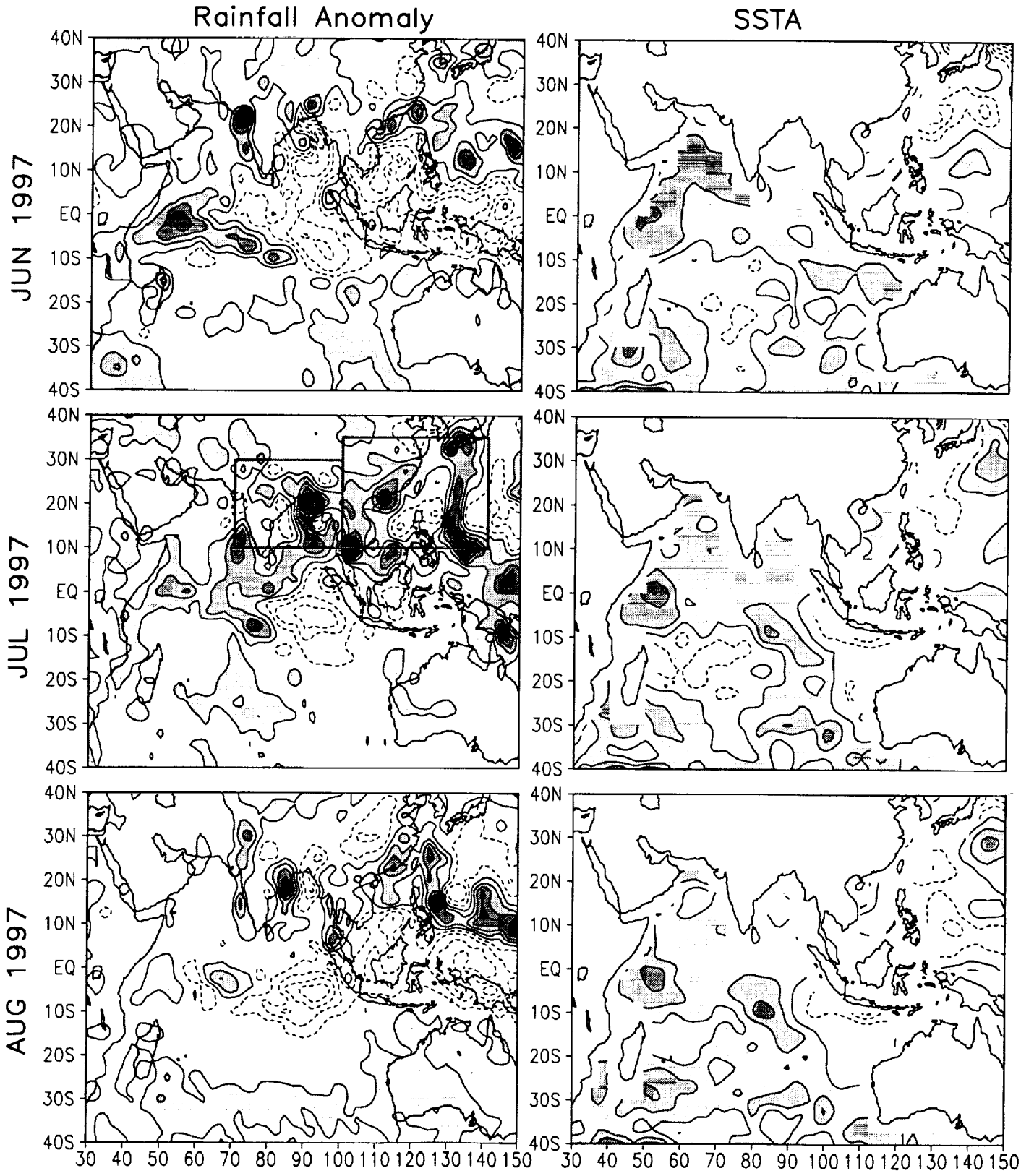
Rainfall Anomaly
SSTA
JUN 1997
JUL 1997
AUG 1997
40N
30N
20N
10N
EQ
10S
20S
30S
40S
30 40 50 60 70 80 90 100 110 120 130 140 150

Fig 1a

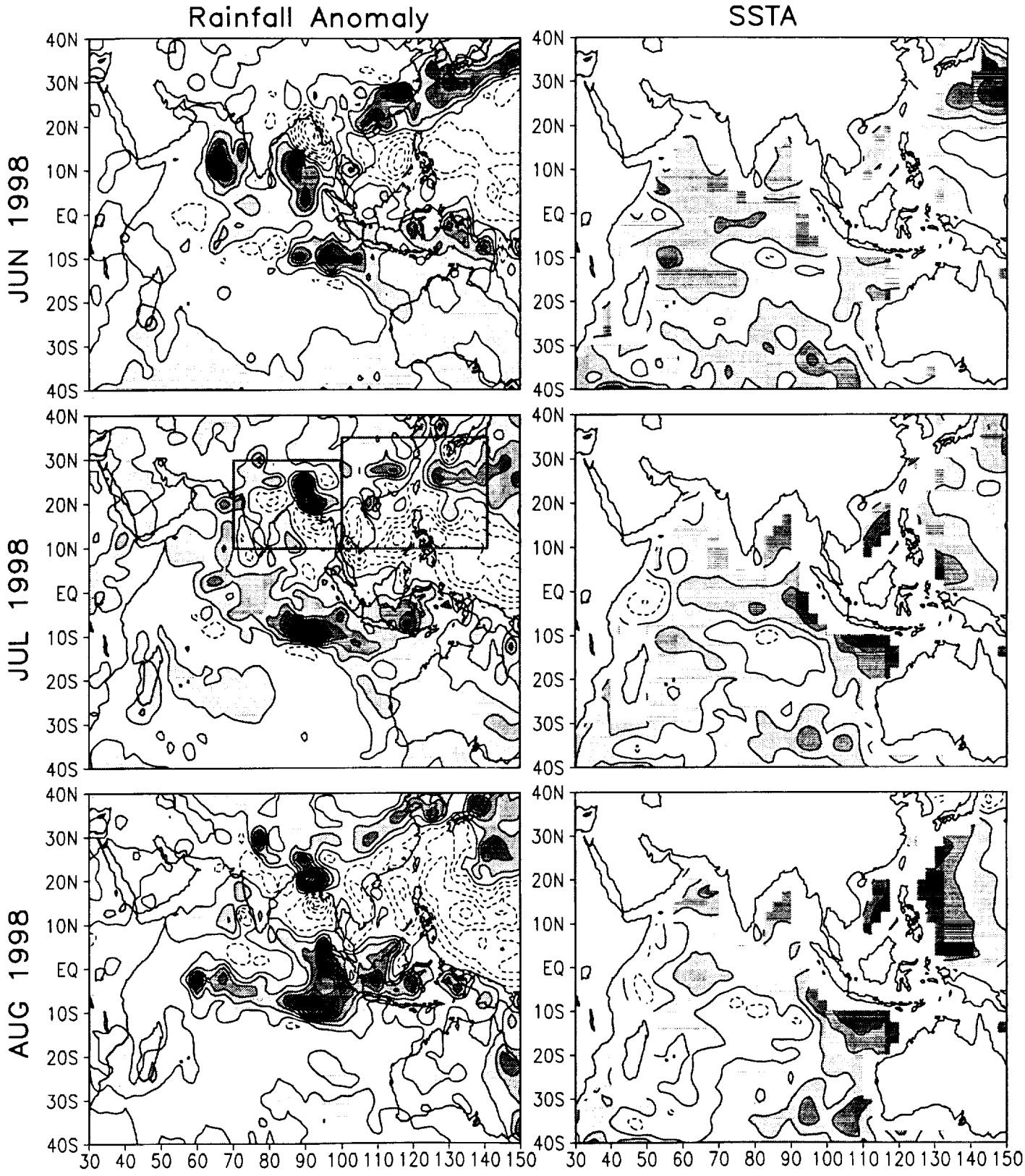
Rainfall Anomaly
SSTA
JUN 1998
JUL 1998
AUG 1998
40N
30N
20N
10N
EQ
10S
20S
30S
40S
30 40 50 60 70 80 90 100 110 120 130 140 150

Fig 16

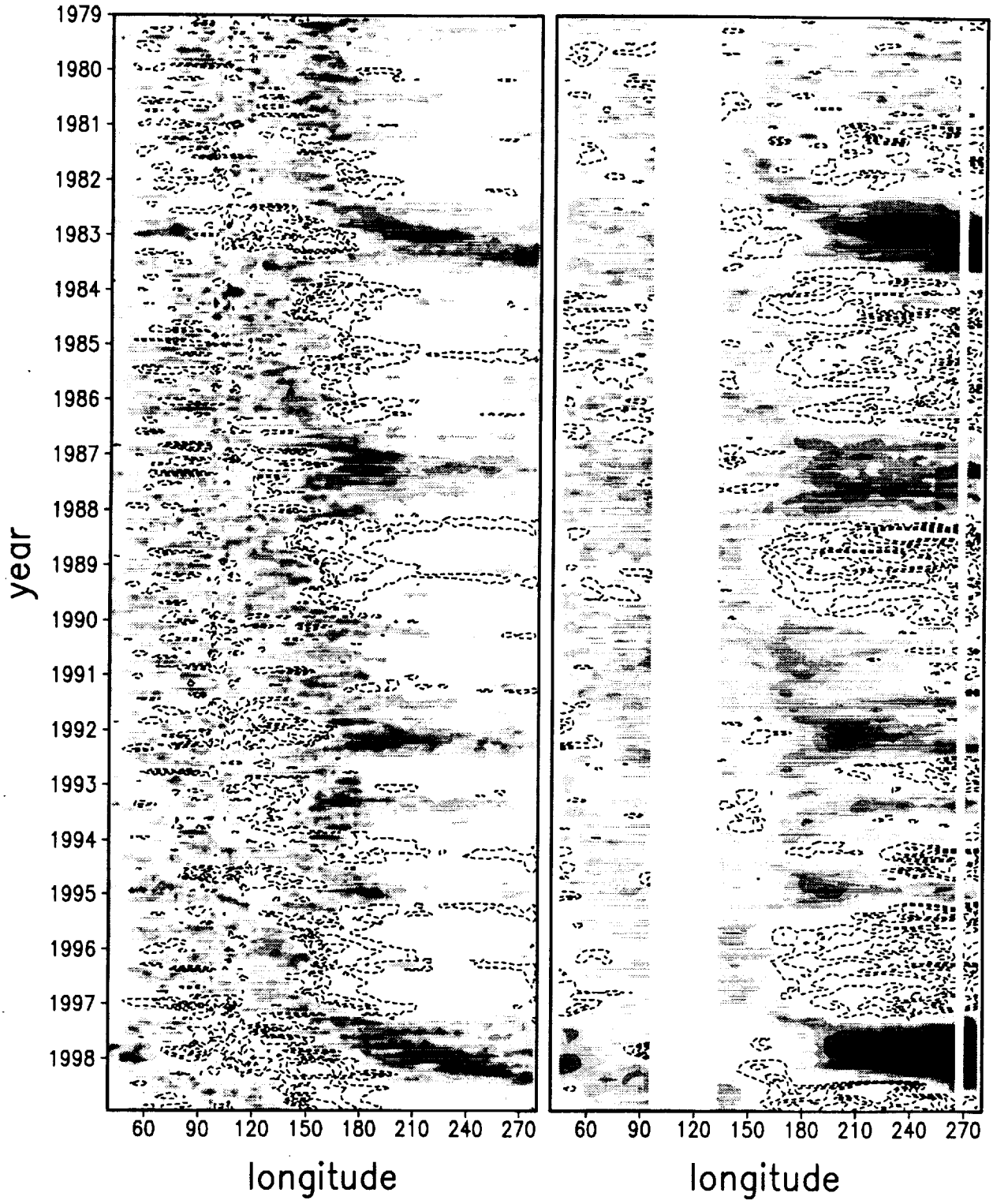
1979
1980
1981
1982
1983
1984
1985
1986
1987
1988
1989
1990
1991
1992
1993
1994
1995
1996
1997
1998
year
60 90 120 150 180 210 240 270
longitude
60 90 120 150 180 210 240 270
longitude

Fig 2

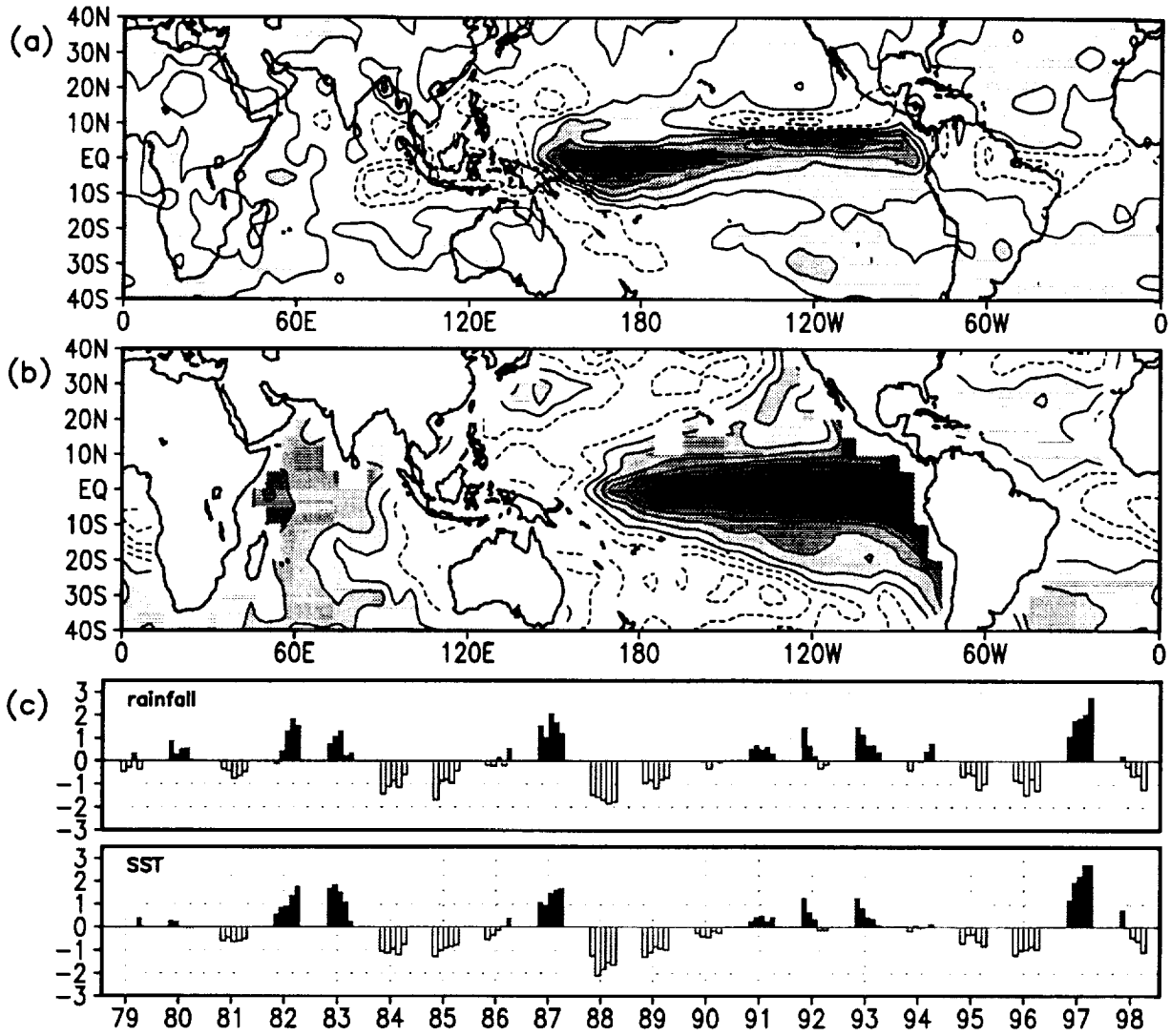
(a)
40N
30N
20N
10N
EQ
10S
20S
30S
40S
0
60E
120E
180
120W
60W
0
(b)
40N
30N
20N
10N
EQ
10S
20S
30S
40S
0
60E
120E
180
120W
60W
0
(c)
rainfall
3
2
1
0
−1
−2
−3
SST
3
2
1
0
−1
−2
−3
79 80 81 82 83 84 85 86 87 88 89 90 91 92 93 94 95 96 97 98

Fig 3

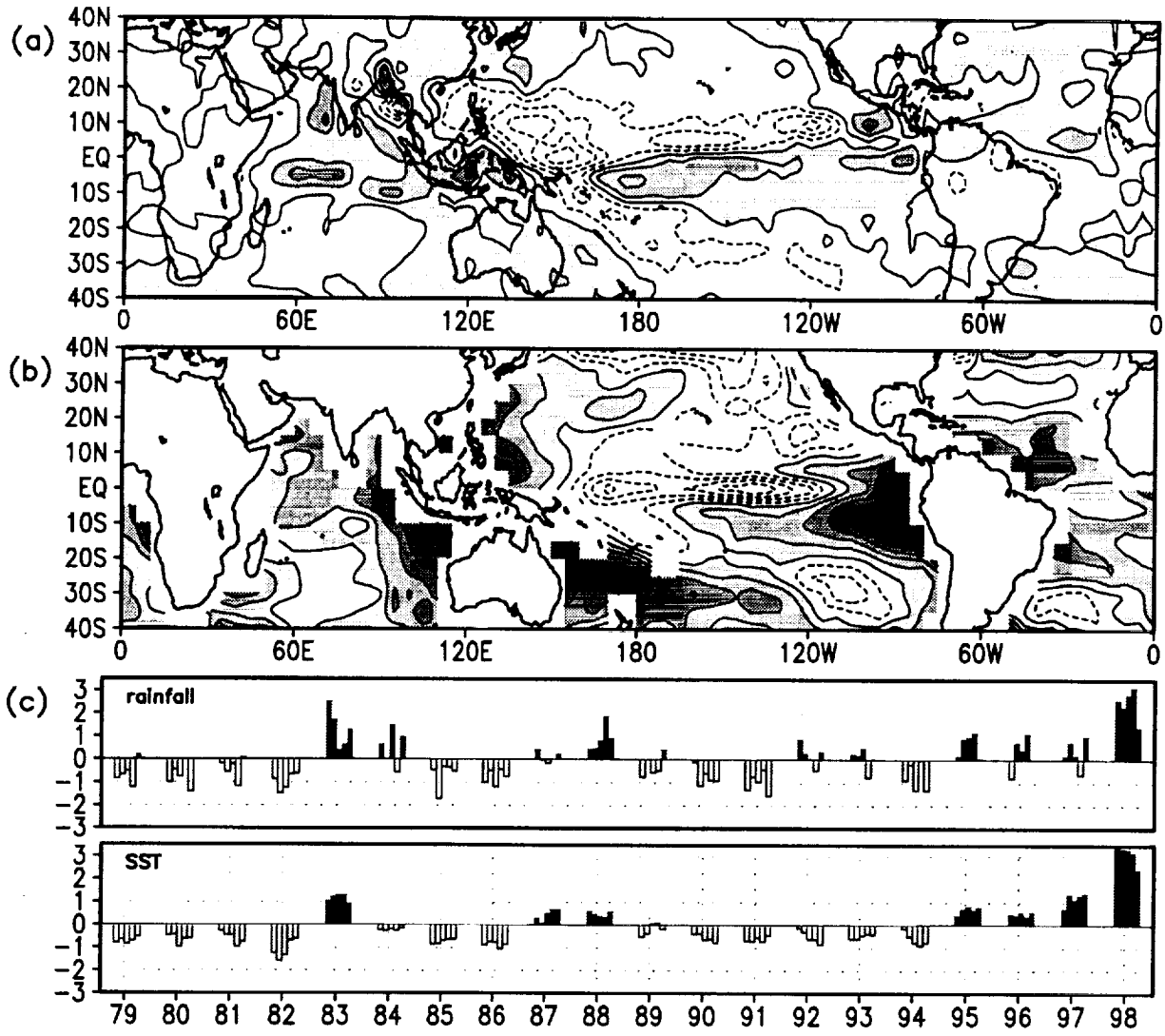
(a)
40N
30N
20N
10N
EQ
10S
20S
30S
40S
0
60E
120E
180
120W
60W
0
(b)
40N
30N
20N
10N
EQ
10S
20S
30S
40S
0
60E
120E
180
120W
60W
0
(c)
rainfall
3
2
1
0
−1
−2
−3
SST
3
2
1
0
−1
−2
−3
79 80 81 82 83 84 85 86 87 88 89 90 91 92 93 94 95 96 97 98

Fig 4

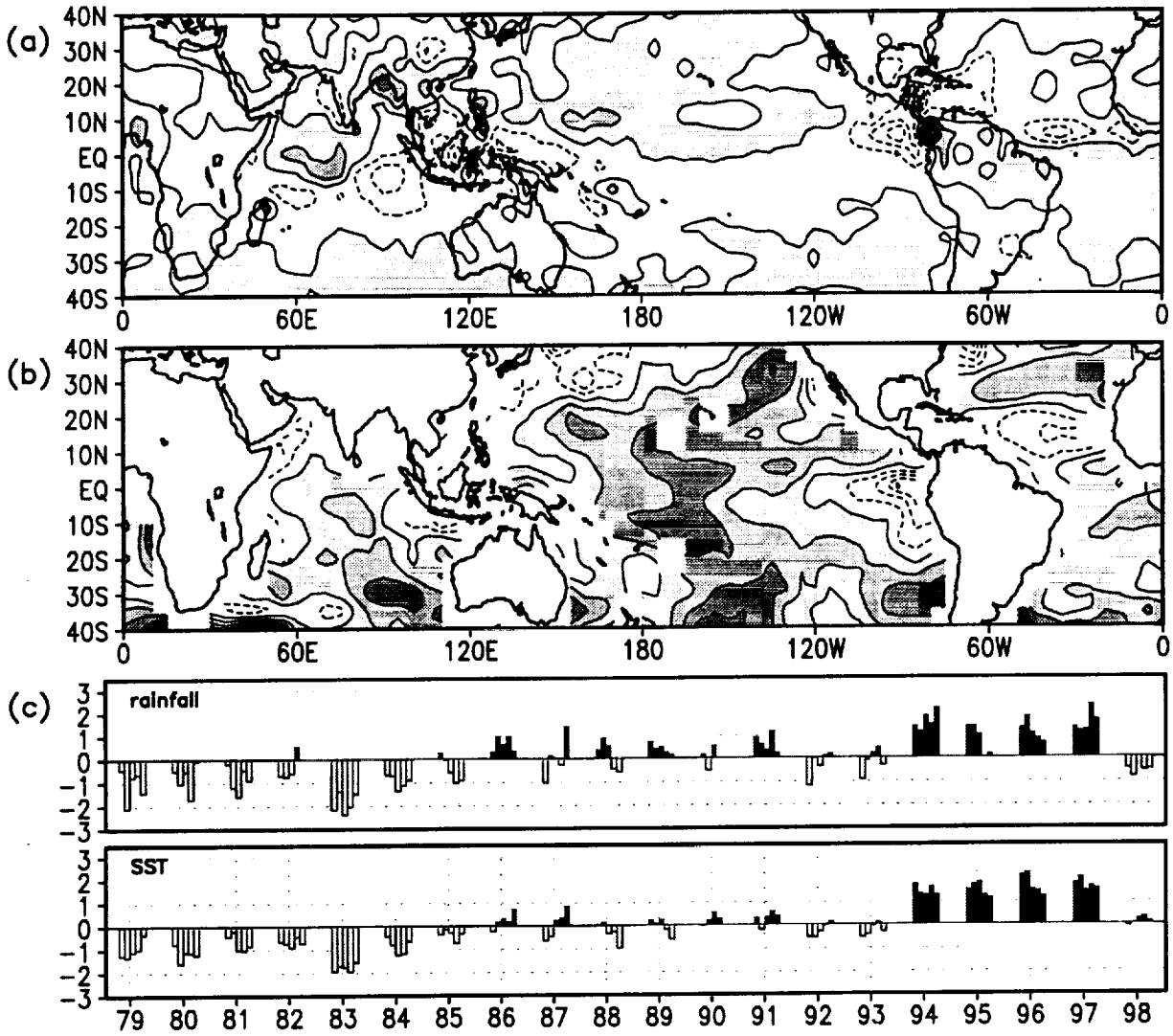
(a)
40N
30N
20N
10N
EQ
10S
20S
30S
40S
0
60E
120E
180
120W
60W
0
(b)
40N
30N
20N
10N
EQ
10S
20S
30S
40S
0
60E
120E
180
120W
60W
0
(c)
rainfall
3
2
1
0
−1
−2
−3
SST
3
2
1
0
−1
−2
−3
79 80 81 82 83 84 85 86 87 88 89 90 91 92 93 94 95 96 97 98

Fig 5

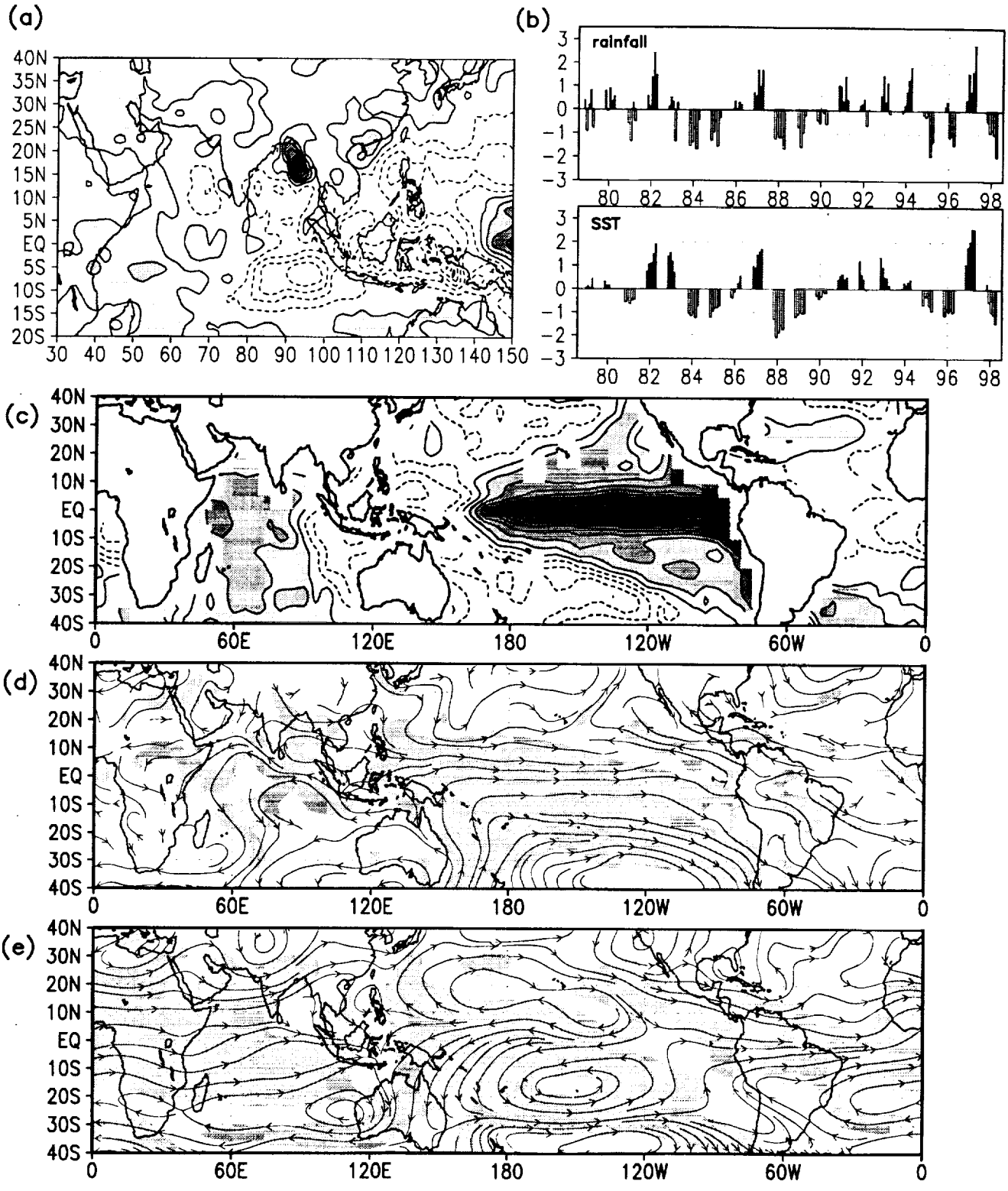
(a)
40N
35N
30N
25N
20N
15N
10N
5N
EQ
5S
10S
15S
20S
30 40 50 60 70 80 90 100 110 120 130 140 150
(b)
rainfall
3 2 1 0 −1 −2 −3
80 82 84 86 88 90 92 94 96 98
SST
3 2 1 0 −1 −2 −3
80 82 84 86 88 90 92 94 96 98
(c)
40N 30N 20N 10N EQ 10S 20S 30S 40S
0 60E 120E 180 120W 60W 0
(d)
40N 30N 20N 10N EQ 10S 20S 30S 40S
0 60E 120E 180 120W 60W 0
(e)
40N 30N 20N 10N EQ 10S 20S 30S 40S
0 60E 120E 180 120W 60W 0

Fig 6

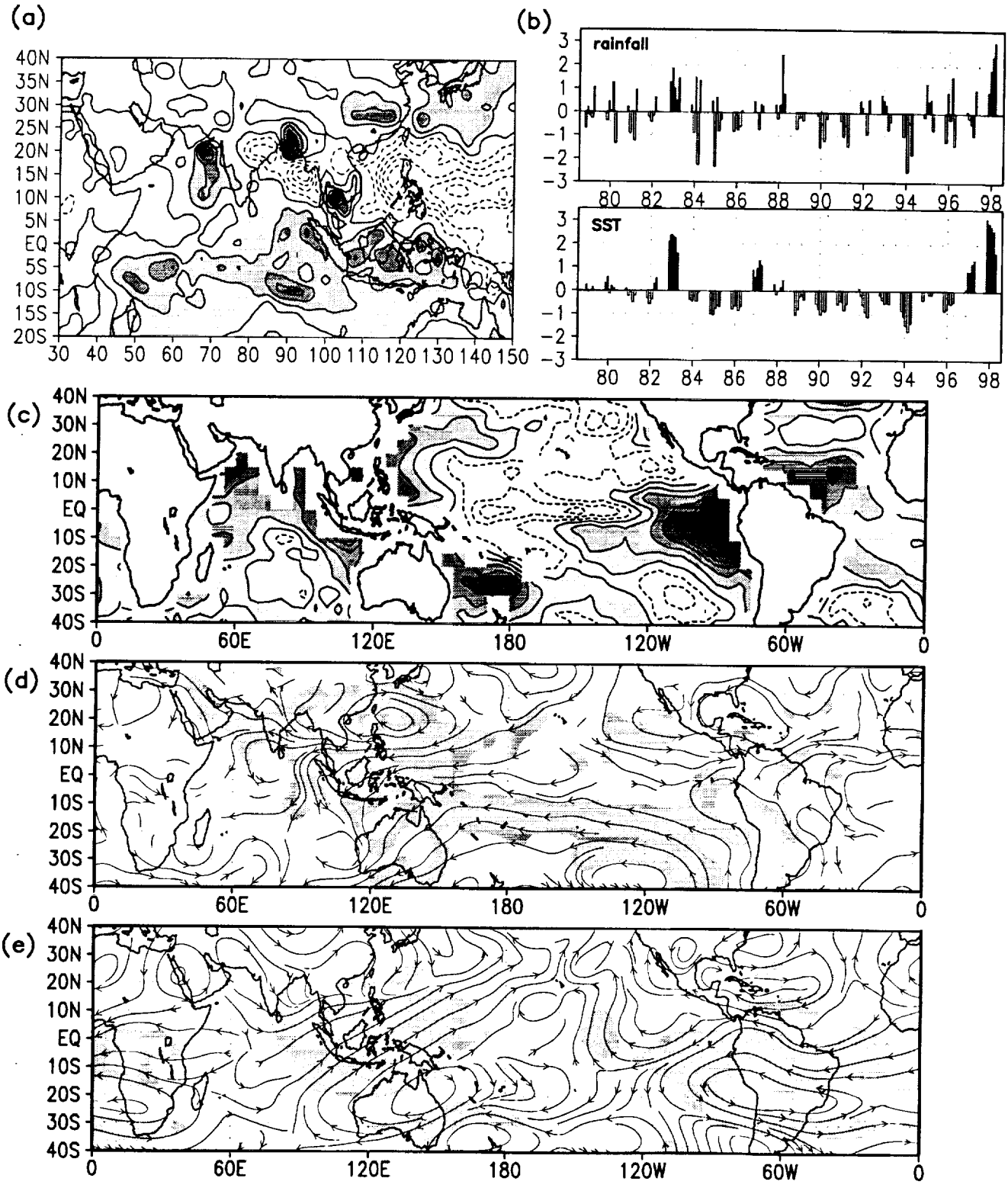
(a)
40N
35N
30N
25N
20N
15N
10N
5N
EQ
5S
10S
15S
20S
30 40 50 60 70 80 90 100 110 120 130 140 150
(b)
rainfall
3 2 1 0 −1 −2 −3
80 82 84 86 88 90 92 94 96 98
SST
3 2 1 0 −1 −2 −3
80 82 84 86 88 90 92 94 96 98
(c)
40N
30N
20N
10N
EQ
10S
20S
30S
40S
0 60E 120E 180 120W 60W 0
(d)
40N
30N
20N
10N
EQ
10S
20S
30S
40S
0 60E 120E 180 120W 60W 0
(e)
40N
30N
20N
10N
EQ
10S
20S
30S
40S
0 60E 120E 180 120W 60W 0

Fig 7

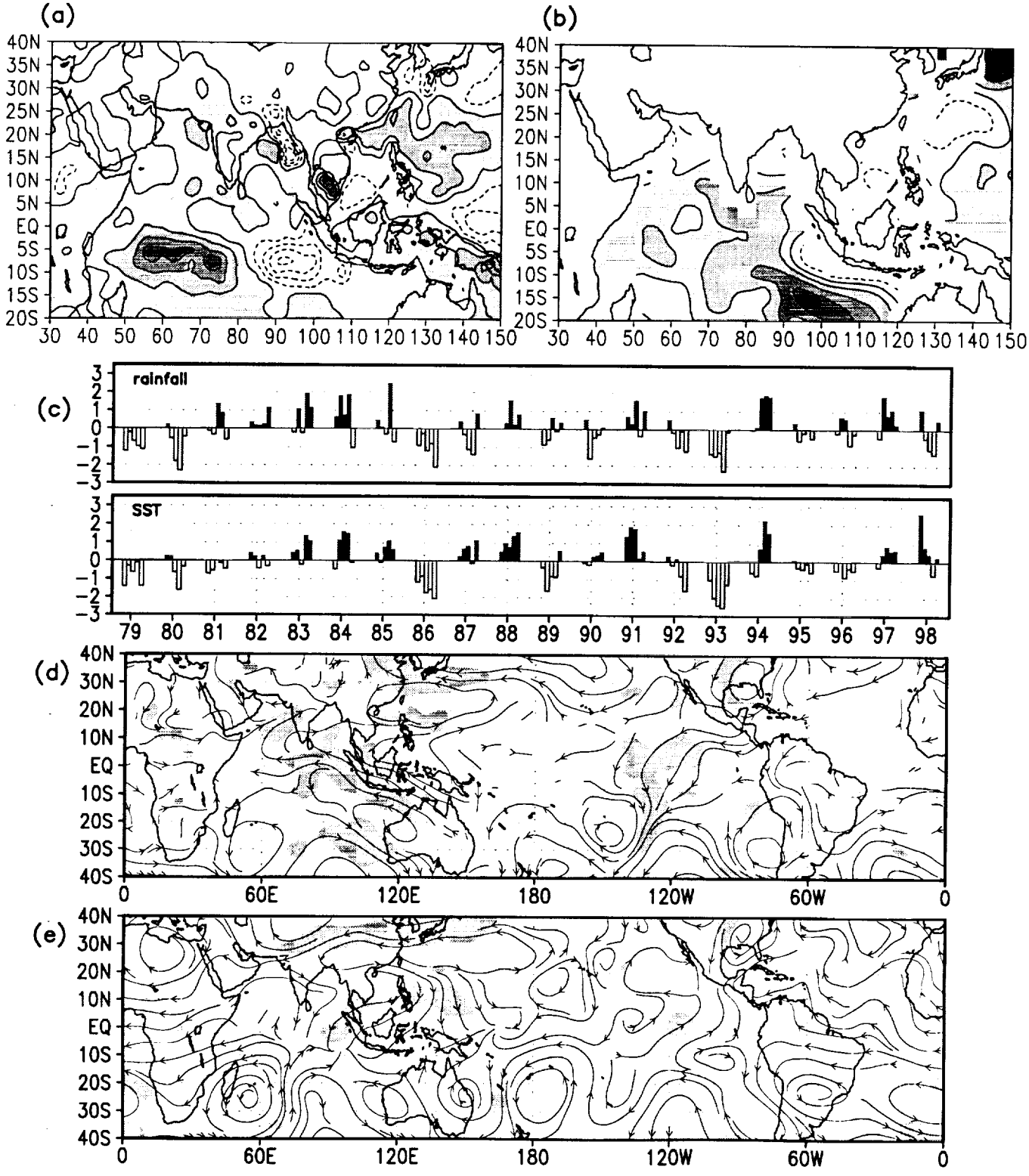
(a)
(b)
(c)
(d)
(e)
rainfall
SST
40N
35N
30N
25N
20N
15N
10N
5N
EQ
5S
10S
15S
20S
30 40 50 60 70 80 90 100 110 120 130 140 150
3
2
1
0
−1
−2
−3
79 80 81 82 83 84 85 86 87 88 89 90 91 92 93 94 95 96 97 98
40N
30N
20N
10N
EQ
10S
20S
30S
40S
0
60E
120E
180
120W
60W
0

Fig 8

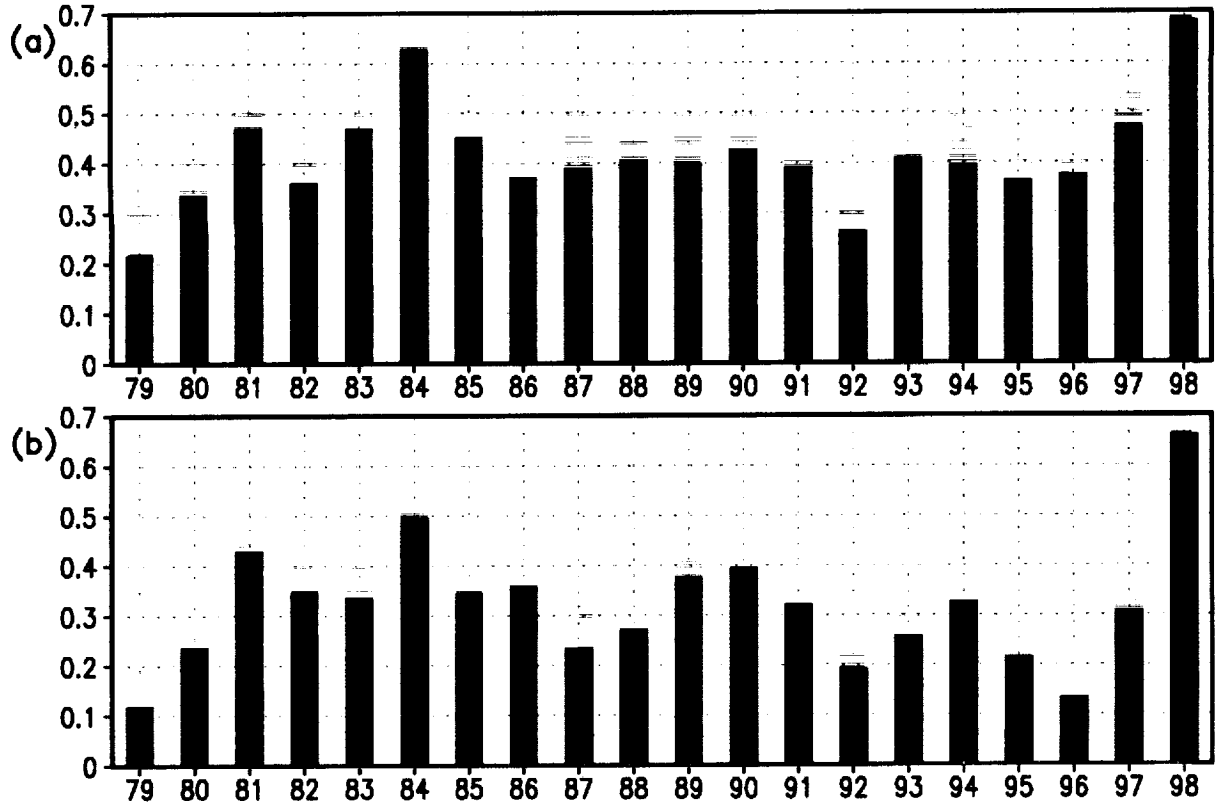
(a)
0.7
0.6
0.5
0.4
0.3
0.2
0.1
0
79 80 81 82 83 84 85 86 87 88 89 90 91 92 93 94 95 96 97 98
(b)
0.7
0.6
0.5
0.4
0.3
0.2
0.1
0
79 80 81 82 83 84 85 86 87 88 89 90 91 92 93 94 95 96 97 98

Fig 9

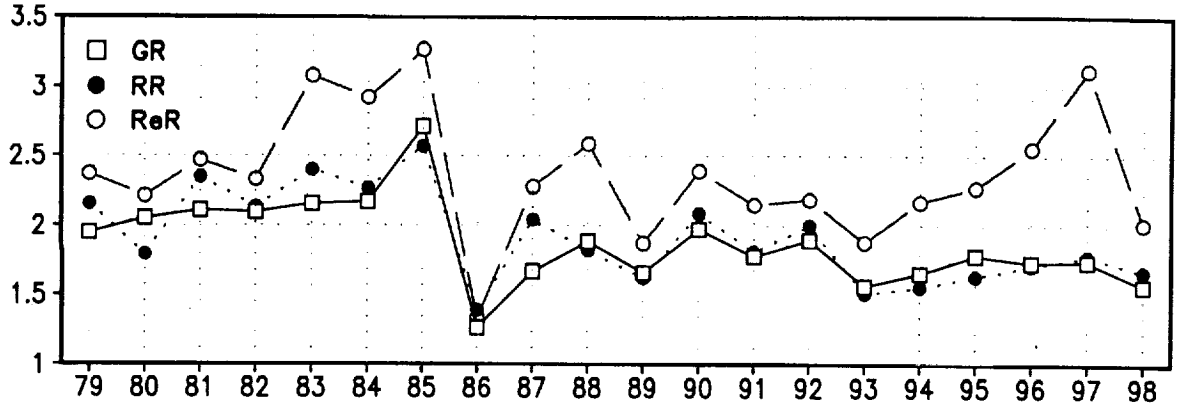
3.5
3
2.5
2
1.5
1
GR
RR
ReR
79 80 81 82 83 84 85 86 87 88 89 90 91 92 93 94 95 96 97 98

Fig 10

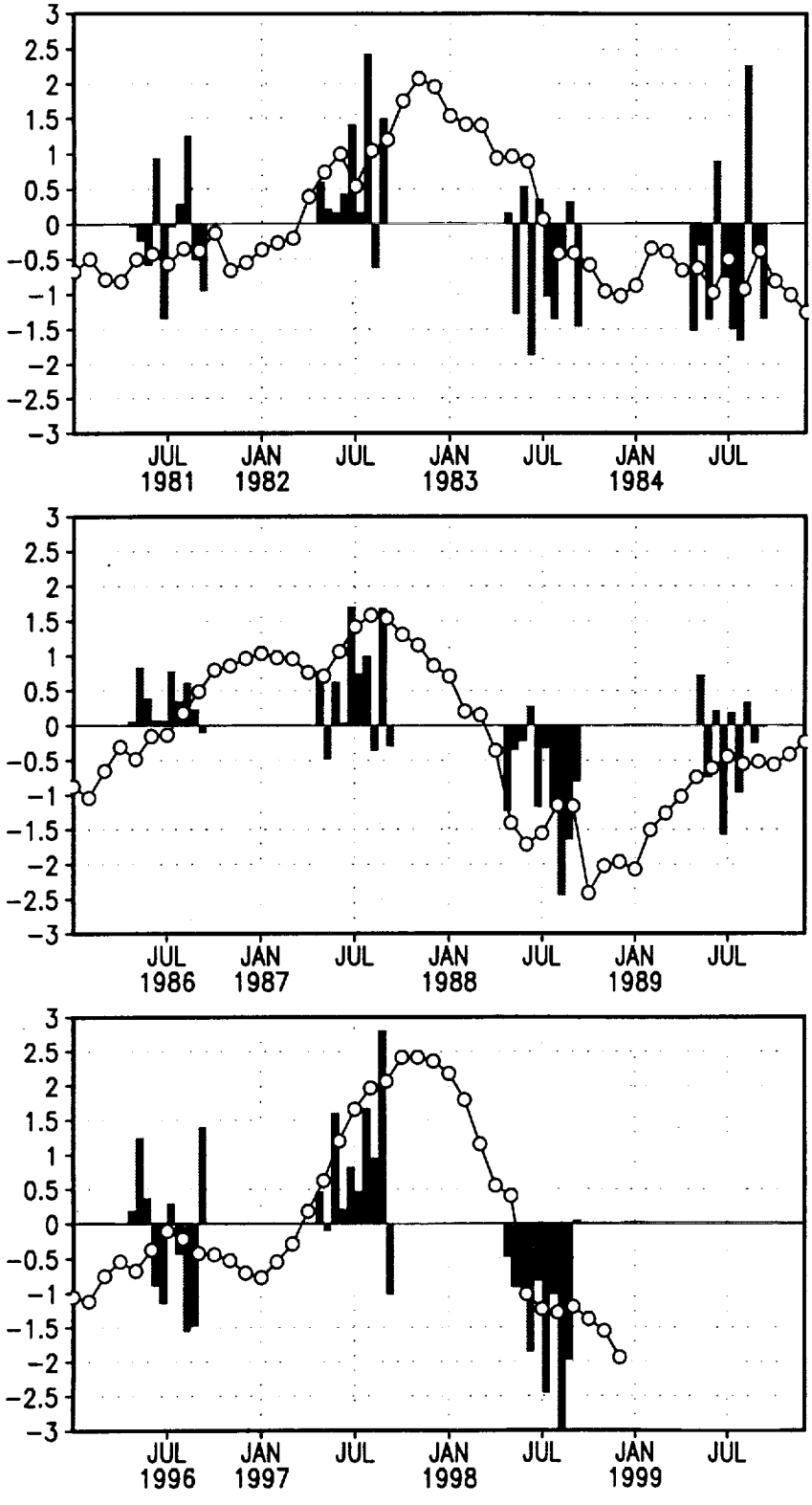
3
2.5
2
1.5
1
0.5
0
−0.5
−1
−1.5
−2
−2.5
−3
JUL 1981
JAN 1982
JUL
JAN 1983
JUL
JAN 1984
JUL
JUL 1986
JAN 1987
JUL
JAN 1988
JUL
JAN 1989
JUL
JUL 1996
JAN 1997
JUL
JAN 1998
JUL
JAN 1999
JUL

Fig 11